HHS Public Access

Author manuscript

Circ Cardiovasc Imaging. Author manuscript; available in PMC 2017 November 27.

Published in final edited form as:

Circ Cardiovasc Imaging. 2016 November ; 9(11): . doi:10.1161/CIRCIMAGING.115.004996.

Persistent Microvascular Obstruction Following Myocardial Infarction Culminates in the Confluence of Ferric Iron Oxide Crystals, Proinflammatory Burden and Adverse Remodeling

Avinash Kali, PhD[1,2,§], **Ivan Cokic, MD**[1,§], **Richard Tang, MD**[1], **Alice Dohnalkova, MS**[3], **Libor Kovarik, PhD**[3], **Hsin-Jung Yang HJ, PhD**[1,2], **Andreas Kumar, MD**[1], **Frank S. Prato, PhD**[4], **John C. Wood, MD, PhD**[5], **David Underhill, PhD**[1,2], **Eduardo Marbán, MD, PhD**[1,2], and **Rohan Dharmakumar, PhD**[1,2]

[1]Cedars-Sinai Medical Center, Los Angeles, CA

[2]University of California, Los Angeles CA

[3]Pacific Northwest National Laboratory, Environmental Molecular Sciences Laboratory, Richland, WA

[4]Lawson Health Research Institute, University of Western Ontario, London, ON, Canada

[5]Children's Hospital Los Angeles, Los Angeles, CA

Abstract

Background—Emerging evidence indicates that persistent microvascular obstruction (PMO) is more predictive of major adverse cardiovascular events than myocardial infarct (MI) size. But, it remains unclear how PMO, a phenomenon limited to the acute/sub-acute period of MI, drives adverse remodeling in chronic MI setting. We hypothesized that PMO resolves into chronic iron crystals within MI territories, which in turn are proinflammatory and favor adverse remodeling post-MI.

Methods and Results—Canines (n=40) were studied with cardiac MRI to characterize the spatiotemporal relationships among PMO, iron deposition, infarct resorption, and LV remodeling between day 7 (acute) and week 8 (chronic) post-MI. Histology was used to assess iron deposition, and to examine relationships between iron content with macrophage infiltration, pro-inflammatory cytokine synthesis, and matrix metalloproteinase activation. Atomic-resolution TEM was used to determine iron crystallinity and energy-dispersive X-ray spectroscopy was used to identify the chemical composition of the iron composite. PMO with or without reperfusion hemorrhage led to chronic iron deposition and the extent of this deposition was strongly related to PMO volume ($r>0.8$). Iron deposits were found within macrophages as aggregates of nanocrystals (~2.5 nm diameter) in the ferric state. Extent of iron deposits was strongly correlated with proinflammatory

*Correspondence to: Rohan Dharmakumar, PhD, Dept of Biomedical Sciences, Cedars-Sinai Medical Center, Biomedical Imaging Research Institute, 8700 Beverly Blvd, PACT Suite 800, Los Angeles, USA 90048, Phone: (310) 423-7641, rohandkumar@csmc.edu.
§Authors contributed equally

Disclosures
None.

burden, collagen degrading enzyme activity, infarct resorption, and adverse structural remodeling (r>0.5).

Conclusions—Crystalized iron deposition from PMO is directly related to proinflammatory burden, infarct resorption, and adverse LV remodeling in the chronic phase of MI in canines. Therapeutic strategies to combat adverse remodeling could potentially benefit from taking into account the chronic iron-driven inflammatory process.

Keywords

persistent microvascular obstruction; hemorrhage; iron deposition; LV remodeling; inflammation; crystals

Infarct size has long known to be an independent predictor of adverse left-ventricular (LV) remodeling in the post myocardial infarction (MI) period [1]. In addition to infarct size, several clinical and pre-clinical studies have shown that the extent of microvascular obstruction (MO) is an important independent predictor of adverse LV remodeling [2–4] Emerging evidence now supports the notion that MO may be more predictive of major adverse cardiovascular events (MACE) than infarct size itself [5, 6]. In spite its importance, how MO, a phenomenon limited to the acute/sub-acute period of MI, imparts adverse remodeling throughout the post-MI period, particularly after its resolution, is not well understood.

Recent studies have shown that MO is frequently accompanied by reperfusion hemorrhage [7, 8] and that it is these types of MIs that remodel the worst and are at the greatest risk for MACE [5, 6, 9]. Serial imaging studies along with histological evidence have shown that reperfusion hemorrhage leads to chronic iron deposition, which is associated with prolonged recruitment of macrophages [10, 11]. However, the physicochemical characteristics of the iron deposits within the infarcted myocardium, the phenotypes of the macrophages in iron-rich infarct regions, and their relation to infarct remodeling or the global structural/functional LV remodeling are not known. Moreover, MO is not always accompanied by acute reperfusion hemorrhage, but infarctions with MOs in the absence of hemorrhage also have significantly poor outcome over infarctions without MO [6]. Thus, even if post-MI iron influences remodeling of hemorrhagic MI in the chronic period, this would not explain the outcomes associated with infarctions with MO but no hemorrhage.

Among the methods used for noninvasively characterizing MO, the hypointense core within late-gadolinium enhancement (LGE) cardiac magnetic resonance imaging (CMR) at 7–10 days post-MI (referred below as persistent (late) MO, PMO) has emerged as a reliable means for detecting MOs that are most significantly associated with adverse outcomes [5, 6, 9]. In this study we investigated the fate of acute MIs with PMO (with and without reperfusion hemorrhage) in the chronic phase to elucidate the interplay between (a) the compositional changes in PMO territories; (b) inflammatory response; and (c) adverse remodeling of infarct zone and LV. Specifically, we hypothesized that (a) every PMO (with or without reperfusion hemorrhage) resolves into crystallized iron in ferric state with the amount of iron deposition dependent on the size of PMO; and (b) the magnitude of iron deposition is related to proinflammatory burden and is a potent, independent factor influencing adverse infarct

and LV remodeling. To systematically examine our hypothesis, we used two canine models of infarction with PMO (with and without hemorrhage) and serial CMR to characterize the spatiotemporal relationships among PMO, iron deposition, and infarct and LV remodeling indices. We used histopathology to a) validate the iron deposition; and b) to study the relationship between iron-rich chronic MI regions against proinflammatory macrophages, cytokines, and collagen degradation. In addition, we used atomic resolution transmission electron microscopy (TEM) to determine the crystallinity of iron and assess the physical effects of iron on macrophages, and energy-dispersive X-ray spectroscopy (EDS) to identify the chemical composition of the iron composite.

METHODS

Animal Preparation and CMR Protocol

Canines (n=40) were studied according to the protocols approved by the Institutional Animal Care and Use Committee. Left lateral thoracotomies were performed and the LAD was ligated at 1.0–1.5cm distal to the bifurcation of the left main coronary artery. A Doppler ultrasound probe (Crystal Biotech, Northborough, MA, USA) was secured 2.0–2.5cm distal to the LAD ligation and no-flow occlusion was confirmed by the absence of blood flow in the distal coronary segment. Ischemia was confirmed by pale blue coloration of the LAD territory following ligation. In 20 canines (Non-Reperfused group), the LAD was permanently ligated and the canines were allowed to recover after closing the chest cavities. In the remaining 20 canines (Reperfused group), ischemia-reperfusion injury was induced by releasing the ligation after 3 hours and re-establishing blood flow in the LAD as confirmed by Doppler blood flow measurements. All canines underwent CMR at 7 days (acute) and 56 days (chronic) post-MI (see Supplement 1 for study timeline) on a 3T clinical MRI system (MAGNETOM Verio, Erlangen, Siemens Healthcare). ECG-triggered breath-held 2D Cine-SSFP, T2*-weighted, and Late Gadolinium Enhancement (LGE) images were acquired (see Supplement 2 for imaging parameters). Animals were euthanized following the day 56 CMR scan and their hearts were excised for ex-vivo tissue examination.

CMR Image Analyses

All CMR image analyses were performed on cvi^{42} image processing software (Circle Cardiovascular Imaging Inc., Calgary, AB, Canada). LV structural remodeling was quantified using end-diastolic sphericity index (EDSI) measurements from cine-SSFP images (14). LV functional remodeling was quantified using end-diastolic volume (EDV), end-systolic volume (ESV), and ejection fraction (EF) measurements from cine-SSFP images normalized to the body surface area. Percentage change in the LV structure and function parameters (ΔEDSI, ΔEDV, ΔESV, and ΔEF) between the acute and chronic phases post-MI were also calculated.

Semi-automatic thresholding was used to identify infarcted myocardium and PMO from LGE images (see Supplement 3 for additional details). For the sake of simplicity, the classic PMO arising from the no-reflow phenomenon in reperfused MIs is henceforth referred to as PMO, while the PMO observed on the day 7 LGE images in non-reperfused MIs is referred to as NR-PMO (non-reperfused persistent microvascular obstruction). Hypointense regions

on T2*-weighted images confined to the hyperintense LGE territory, indicative of iron arising from blood degradation within infarcted myocardium, were quantified using semi-automatic thresholding (for thresholds, see Supplement 3).

Based on the presence or absence of PMO and iron within the infarcted territories at 7 days post-MI, canines from both the Reperfused and Non-Reperfused groups were classified as $PMO^{+}/T2^{*+}$ (both PMO and T2* loss were present), $PMO^{+}/T2^{*-}$ (PMO was present but T2* loss was absent), $PMO^{-}/T2^{*+}$ (PMO was absent but T2* loss was present), and $PMO^{-}/T2^{*-}$ (both PMO and T2* loss were absent); the prefix NR was used to distinguish the Non-Reperfused groups from the Reperfused groups. Infarct, PMO, and iron volumes were calculated at both acute and chronic phases across all the groups as the percentage of total LV myocardial volume. Infarct resorption was quantified as the absolute change in infarct volume normalized to LV volume (%LV) between acute and chronic phases. T2* values of the remote myocardium, entire infarcted myocardium, and the iron deposits within the infarcted myocardium were also measured.

Histopathological Validation and Quantification of Inflammatory Burden and Collagen Degradation

Freshly explanted hearts from the canines were sectioned along the short-axis direction from base to apex into 1-cm thick slices. Infarcted and remote territories were identified on the basis of TTC staining. Ex-vivo 2D T2*-weighted images (same parameters were used as those for the in-vivo images) were subsequently acquired from the slices positive for MI on TTC staining. Based on the presence of hypointense cores within the infarcted territories on the ex-vivo T2*-weighted images, slices were classified as those with and without iron deposition (T2*+ and T2*− respectively). Paraffin-embedded serial sections (5 μm) from representative segments of infarcted and remote areas were stained with H&E stain for necrosis, EMT stain for fibrosis, and Perl's stain for iron deposition. For immunostaining, sections were probed with antibodies against the markers of newly recruited neutrophils and monocytes (Mac387), iron-specific (CD163) and proinflammatory macrophages (those expressing inflammatory cytokines, IL-1β, and TNF-α) and matrix metalloprotinease (MMP-9) (see Supplement 4 for additional details). Quantitative histological analyses were performed from representative histologic sections with TTC evidence of MI from 10 reperfused and 10 non-reperfused animals, following digitization of slides on ScanScope AT (Aperio Technologies, Vista, CA). Morphometric analysis was performed using Definiens Tissue Studio (Definiens, Parsippany, NJ) software. Predefined stain-specific algorithms and classification tools were created utilizing Definiens eCognitionNetwork Language™ to identify positive and negative stained area under the marker (for every 1 μm^2) within each tissue region in an automated fashion to reduce operator bias. Thresholds were set to classify the following: blue for iron, and DAB stain for Mac387, CD163, IL-1β, TNF-α, and MMP-9.

Transmission Electron Microscopy, Atomic Resolution Imaging and Energy-Dispersive X-ray Spectroscopy (EDS)

Samples positive for iron from ex-vivo sections were further dissected into 1 mm^3 cubes and fixed in 2.5% glutaraldehyde (Electron Microscopy Sciences (EMS), Hatfield, PA) and

processed by washing them with dH_2O, and a gradual dehydration by using ethanol series (25%, 33, 50, 75, and 3× 100% ethanol). The traditional stains for contrast enhancement such as OsO_4 were purposely omitted to preserve the redox state of the biominerals. Samples were then infiltrated in LR White acrylic resin (EMS), and polymerized at 60 °C for 24 hours. The hardened resin blocks were sectioned on a Leica EM UC6 ultra-microtome using a 45° diamond knife (DiATOME, Hatfield, PA). 70-nm thick sections were collected on copper grids coated with ultrathin carbon film on holey carbon support film (Ted Pella, Inc., Redding, CA) and imaged on a Tecnai T-12 TEM (FEI, Hillsboro, OR) with a LaB6 filament, operating at 120 kV. Images were collected digitally with a 2×2K Ultrascan 1000 CCD (Gatan, Pleasanton, CA). For the atomic resolution imaging, the previously identified areas of interest were correlatively imaged using Titan S/TEM (FEI, Hillsboro, OR), operating at 300kV. The diffraction patterns of the nanocrystalline material were collected while operating S/TEM in the selected area electron diffraction (SAED) mode, to identify the mineral crystallinity. The chemical elemental analysis was performed with energy dispersive spectroscopy, using a Si(Li) detector (EDAX, Mahwah, NJ), coupled to the STEM.

Statistical Analyses

All statistical analyses were performed using IBM SPSS Statistics (version 21.0, IBM Corporation, Armonk, NY). Since the within-group sample sizes were less than 20 in this study, we have used non-parametric tests for all comparisons. Mann-Whitney U test was used to compare independent samples, and Wilcoxon signed rank test was used for pairwise comparisons. Univariable and multivariable linear regression analyses were performed to determine the associations among different measurement variables. Statistical significance was set at $p<0.05$. All data is expressed as Median with first and third quartiles.

RESULTS

None of the data presented here is from our previous work[10]. Three canines within the Reperfused group and four canines from the Non-Reperfused group died within the first week post-MI. The remaining 17 canines from the Reperfused group and 16 canines from the Non-Reperfused group sustained MIs as confirmed by LGE images on day 7. These animals were followed up to 56 days post-MI.

Persistent Microvascular Obstruction Leads to Iron Deposition within Chronic MI

In the Reperfused group, 9 canines were classified as $PMO^+/T2^{*+}$, 4 canines were classified as $PMO^+/T2^{*-}$, and 4 canines were classified as $PMO^-/T2^{*-}$ at 7 days post-MI. No canine was classified as $PMO^-/T2^{*+}$ on day 7 post-MI. Representative T2*-weighted and LGE images from the $PMO^+/T2^{*+}$, $PMO^+/T2^{*-}$, and $PMO^-/T2^{*-}$ groups in both acute and chronic phases are shown in Figure 1, along with corresponding ex-vivo histology sections stained with TTC, EMT, and Perl's stains. No PMO could be observed on LGE images in all the 3 groups in the chronic phase. In the $PMO^+/T2^{*+}$ group, significant T2* losses indicative of iron deposition could be visually observed in all the canines within the infarcted territories in both acute and chronic phases. While none of the canines in the $PMO^+/T2^{*-}$ showed T2* losses within the infarct in the acute phase, all the canines subsequently showed

significant T2* losses within the infarct in the chronic phase. None of the canines in the $PMO^{-}/T2^{*-}$ group showed any T2* losses within the infarct in both acute and chronic phases. TTC images confirmed the presence of infarction in all the groups (Figure 1). Perls staining validated the presence of iron deposition in the chronic phase in the $PMO^{+}/T2^{*+}$ and $PMO^{+}/T2^{*-}$ groups, and the absence of iron deposition in the $PMO^{-}/T2^{*-}$ group (Figure 1).

In the Non-Reperfused group, 15 canines were classified as NR-$PMO^{+}/T2^{*+}$, and 1 canine was classified as NR-PMO^{-}/ $T2^{*-}$. No canine was classified as either NR-PMO^{+}/ $T2^{*-}$ or NR-$PMO^{-}/T2^{*+}$ on day 7 post-MI. Representative T2*-weighted and LGE images from the NR-$PMO^{+}/T2^{*+}$ and NR-$PMO^{-}/T2^{*-}$ groups in both acute and chronic phases are shown in Figure 2, along with corresponding ex-vivo histology sections stained with TTC, EMT, and Perl's stains. No PMO could be observed on LGE images in both the groups in the chronic phase. In the NR-PMO^{+}/ $T2^{*+}$ group, significant T2* losses indicative of iron deposition could be visually observed in all the canines within the infarcted territories in both acute and chronic phases. The only canine in the NR-$PMO^{-}/T2^{*-}$ group did not show any T2* loss within the infarct in both acute and chronic phases. TTC images confirmed the presence of MI in all the groups (Figure 2). Perls staining validated the presence of iron deposition in the chronic phase in the NR-$PMO^{+}/T2^{*+}$ group, but not in the NR-$PMO^{-}/T2^{*-}$ group.

Extent of Chronic Iron Deposition is Strongly Related to Acute PMO Volume in Reperfused and Non-Reperfused MIs

In the Reperfused group, median acute PMO volume in the $PMO^{+}/T2^{*+}$ group was higher than that of the $PMO^{+}/T2^{*-}$ group ($p=0.03$, Figures 3A). PMO completely resolved in the chronic phase in both $PMO^{+}/T2^{*+}$ and $PMO^{+}/T2^{*-}$ groups. Relative to the acute phase, median iron volume in the chronic phase decreased in the $PMO^{+}/T2^{*+}$ group ($p=0.02$; Figure 3B). In contrast, median iron volume in the $PMO^{+}/T2^{*-}$ group increased from 0 in the acute phase to 2.6 (1.8–3.2) ($p=0.04$; Figure 3B). Significant relationships were observed between the PMO volume and acute iron volume ($R^2=0.40$, $p<0.001$; Figure 3C), and PMO volume and chronic iron volume ($R^2=0.73$, $p<0.001$; Figure 3C).

In the Non-Reperfused group, NR-PMO resolved completely in the chronic phase (Figure 3D). No significant difference was observed between median acute and chronic iron volumes in the NR-$PMO^{+}/T2^{*+}$ group ($p=0.06$; Figure 3E). Significant relationships were observed between the NR-PMO volume and acute iron volume ($R^2=0.86$, $p<0.001$; Figure 3F), and NR-PMO volume and chronic iron volume ($R^2=0.66$, $p<0.001$; Figure 3F).

Iron Accumulates within Chronic Infarction Territories as Nanocrystals

TEM of chronic MI sections, positive for iron in ex-vivo T2* CMR, revealed the presence of electron dense materials within macrophages that were organized into nodules (~200 nm in diameter; Figure 4). The individual nodules were found to be aggregates of highly crystalline nanoparticles (~ 2.5-nm in diameter). Specifically, the aggregates were enclosed by spherically shaped organelles suggestive of lysosomes (see Figure S1 in Supplement 5). S/TEM of the particulate material showed a highly ordered atomic pattern, and the EDS spectrum revealed a strong presence of iron. The EDS confirmed the diffraction pattern

(with diffraction rings at 0.150 nm, 0.176 nm, 0.214 nm, 0.226 nm, and 0.256 nm) to be an exact fit to the 6-line hydroxy ferrihydrite (Figure 5), which has the chemical formula of $Fe_2O_3 \bullet 0.5H_2O$.

Iron Content, Proinflammatory Burden, and Collagen Degradation are Highly Correlated

Representative microscopic immunohistological sections of reperfused and non-reperfused MIs obtained from canines with and without T2* losses ($T2^{*+}$ and $T2^{*-}$ respectively) as observed on ex-vivo T2*-weighted images are shown in Figure 6. Significant collagen deposition within the infarcted territories could be observed in all cases, while Perl's stain confirmed the presence of iron deposition only in the $T2^{*+}$ cases. Significant co-localization of Mac387+ cells with iron deposits was observed in both reperfused and non-reperfused MIs. There was intense IL-1β and TNF-α immunoreactivity associated with Mac387+ cells. Regression analyses showed strong associations of area of iron (Perl's stain) with area of Mac387+ cells (R^2=0.87, p<0.001; Figure 6A), CD163+ cells (R^2=0.66, p<0.001; Figure 6B), IL-1β activity (R^2=0.58, p<0.001; Figure 6C), TNF-α activity (R^2=0.77, p<0.001; Figure 6D), and MMP-9 activity (R^2=0.94, p<0.001; Figure 6E).

Iron within Chronic MI is Associated with Adverse Remodeling of Chronic Infarction

Relationship between Iron Volume and Infarct Remodeling—In reperfused MIs, median iron volume calculated as a percentage of the total infarct volume significantly increased between acute and chronic phases in both $PMO^+/T2^{*+}$ (p=0.01) and $PMO^+/T_2{}^{*-}$ groups (p=0.04; Figure 7A). Infarct resorption was linearly related to both acute (R^2=0.45, p<0.001) and chronic iron volumes (R^2=0.79, p<0.001; Figure 7B). In non-reperfused MIs, median iron volume calculated as a percentage of the total infarct volume significantly increased between acute and chronic phases in the NR-$PMO^+/T2^{*+}$ group (p=0.001; Figure 7C). Infarct resorption was linearly related to both acute (R^2=0.28, p<0.001) and chronic iron volumes (R^2=0.27, p<0.001; Figure 7D).

Iron within Chronic MI is Associated with Adverse Structural and Functional LV Remodeling

A. Relationship between Iron Volume and Structural LV Remodeling—In the reperfused MIs, $PMO^+/T2^{*+}$ group had significantly larger EDSI (Figure 8A) compared to $PMO^+/T2^{*-}$ and $PMO^-/T2^{*-}$ groups in both acute ($PMO^+/T2^{*+}$ vs. $PMO^+/T2^{*-}$: p=0.01; $PMO^+/T2^{*-}$ vs. $PMO^-/T2^{*-}$: p=0.19; $PMO^+/T2^{*+}$ vs. $PMO^-/T2^{*-}$: p=0.01) and chronic phases ($PMO^+/T2^{*+}$ vs. $PMO^+/T2^{*-}$: p=0.02; $PMO^+/T2^{*-}$ vs. $PMO^-/T2^{*-}$: p=0.03; $PMO^+/T2^{*+}$ vs. $PMO^-/T2^{*-}$: p=0.007). The $PMO^+/T2^{*+}$ group also had significantly larger EDSI in the chronic phase compared to the acute phase (p=0.008), but there was no significant difference in EDSI between the acute and chronic phases in both $PMO^+/T2^{*-}$ (p=0.42) and $PMO^-/T2^{*-}$ (p=0.71) groups. The $PMO^+/T2^{*+}$ group also had significantly higher ΔEDSI (Figure 8B) between the acute and chronic phases compared to the $PMO^+/T2^{*-}$ (p=0.03) and $PMO^-/T2^{*-}$ groups (p=0.01). Simple linear regression analyses showed significant associations of ΔEDSI with both infarct and iron volumes measured at both acute and chronic phases (Figure 8C – acute infarct: R^2=0.46, chronic infarct: R^2=0.29, Figure 8D – acute iron: R^2=0.29, chronic iron: R^2=0.42, p<0.001 for all cases).

Multivariable regression analyses showed that both infarct and iron volumes measured at both acute (infarct: β=2.02, p=0.002; iron: β=1.57, p=0.02) and chronic phases (infarct: β=3.46, p=0.003; iron: β=4.12, p<0.001) were significant and independent predictors of ΔEDSI.

In the non-reperfused MIs, the NR-PMO^{+}/T_2*$^{+}$ group had significantly larger EDSI compared to the NR-PMO^{-}/T_2*$^{-}$ canine in both acute (p=0.02) and chronic (0.008) phases (Figure 8E). The NR-PMO^{+}/T_2*$^{+}$ canines also had significantly larger EDSI in the chronic phase compared to the acute phase (p=0.004; Figure 8E). Compared to the NR-PMO^{-}/T_2*$^{-}$ canine, the NR-PMO^{+}/T_2*$^{+}$ group had significantly higher ΔEDSI between the acute and chronic phases (p=0.008; Figure 8F). Linear regression analyses showed significant associations of ΔEDSI with both infarct and iron volumes measured at both acute and chronic phases (Figure 8G – acute infarct: R^2=0.53, chronic infarct: R^2=0.40; Figure 8H – acute iron: R^2=0.45, chronic iron: R^2=0.42; p<0.001 for all cases). Multivariable regression analyses showed that both infarct and iron volumes measured at both acute (infarct: β=2.75, p=0.006; iron: β=1.64, p=0.01) and chronic phases (infarct: β=4.16, p=0.002; iron: β=4.81, p<0.001) were significant and independent predictors of ΔEDSI. Additional details on comparisons between reperfused and non-reperfused MIs can be found in Supplement 7.

B. Relationship between Iron Volume and Functional LV Remodeling—In the reperfused MIs, canines in the PMO^{+}/T_2*$^{+}$ group had significantly larger EDV, larger ESV, and lower EF compared to the canines in the PMO^{+}/T_2*$^{-}$ and PMO^{-}/T_2*$^{-}$ groups in both acute and chronic phases (see Supplement 8 for numbers and statistical comparisons). The PMO^{+}/T_2*$^{+}$ group also had significantly larger EDV and ESV, and lower EF in the chronic phase compared to the acute phase. However, there was no significant difference in the functional remodeling parameters between the acute and chronic phases in the PMO^{+}/T_2*$^{-}$ and PMO^{-}/T_2*$^{-}$ groups. Compared to the canines in the PMO^{+}/T_2*$^{-}$ and PMO^{-}/T_2*$^{-}$ groups, canines in the PMO^{+}/T_2*$^{+}$ group had significantly higher ΔEDV, ΔESV, and ΔEF between the acute and chronic phases. Neither infarct volume nor iron volume measured at either acute or chronic phase could significantly predict ΔEDV, ΔESV, or ΔEF.

In the non-reperfused MIs, canines in the NR-PMO^{+}/T_2*$^{+}$ group had larger EDV and ESV, and lower EF compared to the NR-PMO^{-}/T_2*$^{-}$ canine in both acute and chronic phases (see Supplement 8 for numbers and statistical comparisons). The NR-PMO^{+}/T_2*$^{+}$ canines also had significantly larger EDV and ESV in the chronic phase compared to the acute phase. However, there was no significant difference in EF between the acute and chronic phases in the NR-PMO^{+}/T_2*$^{+}$ canines. There was no difference in ΔEDV, ΔESV, and ΔEF between the two groups. Neither infarct volume nor iron volume measured at either acute or chronic phase could significantly predict ΔEDV, ΔESV, or ΔEF. Additional details on comparisons between reperfused and non- reperfused MIs can be found in Supplement 8.

DISCUSSION

In this study, we showed that PMO, with or without reperfusion hemorrhage can lead to significant chronic iron deposition within the infarcted territories, and the extent of chronic iron deposition is strongly related to the extent of PMO observed in the acute phase. In

canines with reperfused MIs, we have shown that PMO can still resolve into iron deposition within the infarcted territories in the chronic phase, even if it is not associated with reperfusion hemorrhage as seen acutely on T2*-weighted images. This was further validated by the occurrence of significant chronic iron deposition within non-reperfused MIs, which are classically known to not have any reperfusion hemorrhage [7]. Using TEM and EDS analysis, we showed that such chronic iron deposits are encapsulated as nanocrystals in ferric state within macrophages in membranous structures resembling lysosomes. We used immunohistochemistry to demonstrate significant proinflammatory burden associated with chronic iron deposition. We also showed that the chronic iron deposition post-PMO resolution is associated with infarct resorption, and is a significant and independent predictor of long-term adverse LV structural remodeling.

Iron Deposits within Reperfused and Non-Reperfused Chronic MI

Recent studies in canines and patients with healed MIs have shown that acute reperfusion hemorrhage resolves into iron deposits within the infarcted tissue up to several months post-reperfusion. However, the possibility of chronic iron deposition in the presence of PMO alone without any concurrent reperfusion hemorrhage has not been previously investigated. While infarct resorption can partly explain the relative increase in iron volume in the $PMO^{+}/T2^{*+}$ group, infarct shrinkage alone does not explain how the $PMO^{+}/T2^{*-}$ MIs, which did not have any acute reperfusion hemorrhage as evidenced by T2*-weighted imaging, eventually had significant iron deposition in the scar tissue in the chronic phase. Although the exact mechanism for this occurrence remains to be investigated, one possibility is that the stagnant blood within the blocked ‘no-reflow’ microvasculature of PMO could gradually degrade. The eventual breakdown of the microvasculature with no-reflow can externalize the degraded stagnant blood into the scar tissue and manifest itself as iron deposits.

The occurrence of chronic iron deposition within non-reperfused MIs has also not been shown previously in the literature, although it is known that PMO is equally prevalent in patients regardless of reperfusion[13]. While the PMO observed in reperfused MIs is attributed to plugging of microvasculature by inflammatory cells, erythrocytes and other microembolic debris[14], the pathological mechanism of PMO observed in non-reperfused MIs could be due to permanently occluded coronary artery that has not been reperfused. Similar to chronic iron deposition arising from PMOs without concurrent hemorrhage in reperfused MIs, the source of chronic iron deposition in non-reperfused MIs with PMO could be gradual degradation of permanently ligated vasculature and externalization of degraded stagnant blood into the scar tissue. Hence, our results suggest that chronic iron deposition is a fingerprint of PMO observed in the acute phase, and could be a potential mechanism through which PMO exerts adverse effects in the long-term.

Crystallized Ferric Iron Deposits and Inflammation

S/TEM, EDS and SAED studies revealed for the first time that the iron deposits within chronic MI are found as nodules composed from nanocrystals of iron in ferric form. Moreover, the TEM images also showed that iron aggregates are located within membrane-enclosed structures, suggestive of lysosomes that appear to be loaded to their physical limits

(diameter > 1μm). These findings, along with evidence from previous studies, may help to explain the proinflammatory burden in chronic MI with iron deposits.

Lysosomes are membrane bound spherical organelles, which are rich in hydrolytic enzymes and are typically less than 1 μm in diameter. Disruption of these membranes, due to excessive uptake of hard/sharp crystalline material similar to iron deposits we characterized here, is known to be a key contributor to several inflammatory disease processes[15]. Studies have shown that such disruptions can set forth cascading inflammatory responses. Ferric iron is known to impart oxidative stress through Fenton pathway leading to activation of inflammasomes and up regulation of proinflammatory cytokines (IL-1β and TNF-α)[15]. Specifically, in vitro studies have demonstrated that macrophages incubated with iron activates NF-κB inflammasome, a key transcription factor promoting the expression of proinflammatory cytokines IL-1β and TNF-α. Other in vitro studies have shown that the extent of proinflammatory cytokine expression is dependent on iron concentration[16]. Given our observations that the extent of inflammatory cytokines were closely related to extent of iron burden (Figure 6), in light of the existing prior mechanistic studies in the literature, it appears that that iron overloading within the macrophages may be a key mechanism by which the inflammatory response is perpetuated within chronic infarctions with a prior history of PMO. Additional studies are needed to confirm this potential mechanism.

Proinflammatory Burden and Adverse Remodeling

Chronic iron deposition within reperfused MIs has been previously implicated in adverse LV remodeling [10] and arrhythmogenesis in healed MIs[17]. In line with previous observations, our study has shown that iron deposition post-PMO resolution is a strong predictor of LV structural remodeling. The role of iron in the onset of adverse LV remodeling and heart failure is well documented in non-ischemic iron-overload cardiomyopathies[18,19]. While the exact mechanism by which iron deposition following PMO resolution in MIs mediates adverse LV remodeling remains to be investigated in vivo, active and prolonged proinflammatory activity co-localized with iron deposits with chronic infarctions observed in this study seems to be one potential mechanism. We found significant co-localization of Mac387+ cells with post-PMO iron deposition in the chronic infarcted territories, which is similar to earlier observations in chronic reperfused MIs that sustained acute reperfusion hemorrhage[10]. We also found that the extent of iron deposition is directly proportional to the extent of Mac387+ co-localization. The monoclonal antibody Mac387 recognizes three calgranulins (calcium-binding proteins), which are found in newly recruited myeloid cells, but the immunoreactivity of Mac387 is significantly reduced as monocytes mature to macrophages[20]. Frangogiannis *et al* have shown that the number of Mac387+ cells in the infarcted myocardium was significantly reduced at 7 days post-reperfusion, and this marker can be used an index for new recruitment of leukocytes in the heart[21]. Our finding of the presence of Mac387+ cells to be highly co-localized with iron and iron scavenger receptor CD163[22] in this study shows an active and prolonged iron-driven inflammatory process within chronic infarcts that extends well beyond the acute inflammatory stage. The interaction of Mac387+ cells with post-PMO iron remains to be investigated, but since CD163 is a key marker of iron-induced macrophage activation[23], iron phagocytosis with the intention of clearance seem to be a plausible explanation. However, the imaging-guided

evidence of lack of iron clearance in the chronic phase is a notable feature of acute MIs with PMO and may be the means by which long-lasting effects of PMO are felt in the chronic phase of MI.

A number of proinflammatory cytokines, which have been implicated in the development of LV dysfunction and LV remodeling dysfunction are known to be released when monocytes mature into macrophages. We found that Mac387+ cells are associated with significant IL-1β, TNF-α and MMP-9 activities. TNF-α is a well-known proinflammatory cytokine implicated in development of LV dysfunction, LV remodeling and endothelial dysfunction[24]. MMP-9 activity is known to be associated with extracellular matrix degradation and modulating mechanical architecture of the scar[25]. IL-1β has been shown to promote matrix degradation by enhancing MMP synthesis, while reducing collagen deposition[26], and has emerged as an important therapeutic target in the chronic phase post-MI[27]. These previously established mechanisms could potentially explain our findings of the direct relations between iron deposition, IL-1β, TNF-α, MMP9 and infarct resorption. Moreover, these results suggest that the macrophages derived from Mac387+ cells are in an unrestrained proinflammatory M1 activation state that can potentially worsen LV remodeling.

Recent studies have been instrumental in shedding light on the relation between MO and inflammation. These studies have shown that in cases of reperfused MIs with MO, monocyte recruitment is delayed in the acute and sub-acute period; and, in cases where erythrocyte extravasation (hemorrhage) accompanies MO, iron accumulates within the MI territories in the chronic phase and is site of intense macrophage recruitment [11]. Although adequate inflammatory activity is necessary for wound healing, long-term persistence of inflammation is detrimental to the reparative effects. Mechanistically, the extent of LV remodeling in the post-MI period is related to the timely inhibition and resolution of the inflammatory activity[28]. In particular, prolonged inflammation has been shown to impair collagen deposition and scar formation resulting in reduced tensile strength and LV dilatation[28]. Early studies suggest that ineffective suppression of inflammation post-MI is associated with adverse LV remodeling of the heart[29]. The finding that iron deposits within chronic MI plays an intermediary role in wound healing may be of substantial clinical relevance as it can unravel how PMO imparts adverse long-term effects on the infarcted heart and underscore iron as a therapeutic target in post-infarction heart failure. Importantly, our findings indicate that it would be of significant value to re-examine intracellular iron-chelation[30] and anti-inflammatory[31] therapies over a longer period of time (i.e., extending beyond the acute MI phase) in post-MI patients that are stratified on the basis PMO presentation to curb the rate of adverse LV remodeling.

Study Limitations—While this study demonstrated important associative relations, the causal relationships among iron, proinflammatory burden and remodeling (structural and functional) was not investigated. Additional studies are needed to establish these relations. The sample size of our study is modest, which may have precluded us from observing significant associations of functional LV remodeling parameters such as EDV, ESV, and EF with infarct and iron volumes. Nevertheless, we could still observe a clear relationship of EDSI with infarct and iron volumes, which suggests that longer follow ups (e.g. 6 months) may have led to worse functional LV remodeling in animals with iron deposits. This notion

is consistent with previous demonstration in the heart that the structural changes are preceded by functional consequences[32]. Even though our results did not reach statistical significance, we observed a trend towards larger acute MI size in reperfused MIs than non-reperfused MIs (see Supplement 6), but this remains to be further investigated.

CONCLUSIONS

Territories of persistent microvascular obstructions in the acute phase of MI, with or without reperfusion hemorrhage, resolve into iron oxide nanocrystals in ferric state in the chronic phase of MI. The amount of iron deposition is determined by the extent of persistent microvascular obstruction and is directly related to the extent of proinflammatory burden, infarct resorption and adverse LV remodeling in canines. Crystallized iron depositions resolving from PMO might be a contributing source to the adverse remodeling of the heart and a potential therapeutic target in the chronic phase of MI.

Supplementary Material

Refer to Web version on PubMed Central for supplementary material.

Acknowledgments

A part of this research was performed at Environmental Molecular Sciences Laboratory, a national scientific user facility sponsored by the Department of Energy's Office of Biological and Environmental Research, located at the Pacific Northwest National Laboratory. PNNL is operated for DOE by Battelle Memorial Institute under Contract# DE-AC05-76RL0-1830.

Sources of Funding

This work was supported in part by grants from the National Heart, Lung, and Blood Institute (HL091989 and HL133407) to Dr. Dharmakumar.

References

1. Pfeffer MA, Braunwald E. Ventricular remodeling after myocardial infarction. Experimental observations and clinical implications. Circulation. 1990; 81:1161–1172. [PubMed: 2138525]
2. Wu KC, Zerhouni EA, Judd RM, Lugo-Olivieri CH, Barouch LA, Schulman SP, Blumenthal RS, Lima JA. Prognostic significance of microvascular obstruction by magnetic resonance imaging in patients with acute myocardial infarction. Circulation. 1998; 97:765–772. [PubMed: 9498540]
3. van Kranenburg M, Magro M, Thiele H, de Waha S, Eitel I, Cochet A, Cottin Y, Atar D, Buser P, Wu E, Lee D, Bodi V, Klug G, Metzler B, Delewi R, Bernhardt P, Rottbauer W, Boersma E, Zijlstra F, van Geuns RJ. Prognostic value of microvascular obstruction and infarct size, as measured by CMR in STEMI patients. JACC Cardiovasc Imaging. 2014; 7:930–939. [PubMed: 25212799]
4. Hamirani YS, Wong A, Kramer CM, Salerno M. Effect of microvascular obstruction and intramyocardial hemorrhage by CMR on LV remodeling and outcomes after myocardial infarction: a systematic review and meta-analysis. JACC Cardiovasc Imaging. 2014; 7:940–952. [PubMed: 25212800]
5. Ganame J, Messalli G, Dymarkowski S, Rademakers FE, Desmet W, Van de Werf F, Bogaert J. Impact of myocardial haemorrhage on left ventricular function and remodelling in patients with reperfused acute myocardial infarction. Eur Heart J. 2009; 30:1440–1449. [PubMed: 19346229]
6. Eitel I, Kubusch K, Strohm O, Desch S, Mikami Y, de Waha S, Gutberlet M, Schuler G, Friedrich MG, Thiele H. Prognostic value and determinants of a hypointense infarct core in T2-weighted cardiac magnetic resonance in acute reperfused ST-elevation-myocardial infarction. Circ Cardiovasc Imaging. 2011; 4:354–362. [PubMed: 21518773]

7. Garcia-Dorado D, Theroux P, Solares J, Alonso J, Fernandez-Aviles F, Elizaga J, Soriano J, Botas J, Munoz R. Determinants of hemorrhagic infarcts. Histologic observations from experiments involving coronary occlusion, coronary reperfusion, and reocclusion. Am J Pathol. 1990; 137:301–311. [PubMed: 2386198]

8. Robbers LF, Eerenberg ES, Teunissen PF, Jansen MF, Hollander MR, Horrevoets AJ, Knaapen P, Nijveldt R, Heymans MW, Levi MM, van Rossum AC, Niessen HW, Marcu CB, Beek AM, van Royen N. Magnetic resonance imaging-defined areas of microvascular obstruction after acute myocardial infarction represent microvascular destruction and haemorrhage. Eur Heart J. 2013; 34:2346–2353. [PubMed: 23594591]

9. Carrick D, Haig C, Ahmed N, McEntegart M, Petrie MC, Eteiba H, Hood S, Watkins S, Lindsay MM, Davie A, Mahrous A, Mordi I, Rauhalammi S, Sattar N, Welsh P, Radjenovic A, Ford I, Oldroyd KG, Berry C. Myocardial Hemorrhage After Acute Reperfused ST-Segment-Elevation Myocardial Infarction: Relation to Microvascular Obstruction and Prognostic Significance. Circ Cardiovasc Imaging. 2016; 9:e004148. [PubMed: 26763281]

10. Kali A, Kumar A, Cokic I, Tang RL, Tsaftaris SA, Friedrich MG, Dharmakumar R. Chronic manifestation of postreperfusion intramyocardial hemorrhage as regional iron deposition: a cardiovascular magnetic resonance study with ex vivo validation. Circ Cardiovasc Imaging. 2013; 6:218–228. [PubMed: 23403335]

11. Ye YX, Basse-Lusebrink TC, Arias-Loza PA, Kocoski V, Kampf T, Gan Q, Bauer E, Sparka S, Helluy X, Hu K, Hiller KH, Boivin-Jahns V, Jakob PM, Jahns R, Bauer WR. Monitoring of monocyte recruitment in reperfused myocardial infarction with intramyocardial hemorrhage and microvascular obstruction by combined fluorine 19 and proton cardiac magnetic resonance imaging. Circulation. 2013; 128:1878–1888. [PubMed: 24025595]

12. Jansen E, Kyek A, Schafer W, Schwertmann U. The structure of six-line ferrihydrite. Applied Physics a-Materials Science & Processing. 2002; 74:S1004–S1006.

13. Khan JN, Razvi N, Nazir SA, Singh A, Masca NG, Gershlick AH, Squire I, McCann GP. Prevalence and extent of infarct and microvascular obstruction following different reperfusion therapies in ST-elevation myocardial infarction. J Cardiovasc Magn Reson. 2014; 16:38. [PubMed: 24884638]

14. Wu KC. CMR of microvascular obstruction and hemorrhage in myocardial infarction. J Cardiovasc Magn Reson. 2012; 14:68. [PubMed: 23021401]

15. Martinon F, Petrilli V, Mayor A, Tardivel A, Tschopp J. Gout-associated uric acid crystals activate the NALP3 inflammasome. Nature. 2006; 440:237–241. [PubMed: 16407889]

16. Scaccabarozzi A, Arosio P, Weiss G, Valenti L, Dongiovanni P, Fracanzani AL, Mattioli M, Levi S, Fiorelli G, Fargion S. Relationship between TNF alpha and iron metabolism in differentiating human monocytic THP-1 cells. Br J Haematol. 2000; 110:978–984. [PubMed: 11054092]

17. Cokic I, Kali A, Wang X, Yang HJ, Tang RL, Thajudeen A, Shehata M, Amorn AM, Liu E, Stewart B, Bennett N, Harlev D, Tsaftaris SA, Jackman WM, Chugh SS, Dharmakumar R. Iron deposition following chronic myocardial infarction as a substrate for cardiac electrical anomalies: initial findings in a canine model. PLoS One. 2013; 8:e73193. [PubMed: 24066038]

18. Kirk P, Roughton M, Porter JB, Walker JM, Tanner MA, Patel J, Wu D, Taylor J, Westwood MA, Anderson LJ, Pennell DJ. Cardiac T2* magnetic resonance for prediction of cardiac complications in thalassemia major. Circulation. 2009; 120:1961–1968. [PubMed: 19801505]

19. Tanner MA, Galanello R, Dessi C, Smith GC, Westwood MA, Agus A, Roughton M, Assomull R, Nair SV, Walker JM, Pennell DJ. A randomized, placebo-controlled, double-blind trial of the effect of combined therapy with deferoxamine and deferiprone on myocardial iron in thalassemia major using cardiovascular magnetic resonance. Circulation. 2007; 115:1876–1884. [PubMed: 17372174]

20. Rugtveit J, Scott H, Halstensen TS, Norstein J, Brandtzaeg P. Expression of the L1 antigen (calprotectin) by tissue macrophages reflects recent recruitment from peripheral blood rather than upregulation of local synthesis: implications for rejection diagnosis in formalin-fixed kidney specimens. J Pathol. 1996; 180:194–199. [PubMed: 8976880]

21. Frangogiannis NG, Shimoni S, Chang SM, Ren G, Shan K, Aggeli C, Reardon MJ, Letsou GV, Espada R, Ramchandani M, Entman ML, Zoghbi WA. Evidence for an active inflammatory

process in the hibernating human myocardium. Am J Pathol. 2002; 160:1425–1433. [PubMed: 11943726]

22. Sindrilaru A, Peters T, Wieschalka S, Baican C, Baican A, Peter H, Hainzl A, Schatz S, Qi Y, Schlecht A, Weiss JM, Wlaschek M, Sunderkotter C, Scharffetter-Kochanek K. An unrestrained proinflammatory M1 macrophage population induced by iron impairs wound healing in humans and mice. J Clin Invest. 2011; 121:985–997. [PubMed: 21317534]
23. Cairo G, Recalcati S, Mantovani A, Locati M. Iron trafficking and metabolism in macrophages: contribution to the polarized phenotype. Trends Immunol. 2011; 32:241–247. [PubMed: 21514223]
24. Mann DL. Tumor necrosis factor-induced signal transduction and left ventricular remodeling. J Card Fail. 2002; 8:S379–386. [PubMed: 12555149]
25. Ducharme A, Frantz S, Aikawa M, Rabkin E, Lindsey M, Rohde LE, Schoen FJ, Kelly RA, Werb Z, Libby P, Lee RT. Targeted deletion of matrix metalloproteinase-9 attenuates left ventricular enlargement and collagen accumulation after experimental myocardial infarction. J Clin Invest. 2000; 106:55–62. [PubMed: 10880048]
26. Siwik DA, Chang DL, Colucci WS. Interleukin-1beta and tumor necrosis factor-alpha decrease collagen synthesis and increase matrix metalloproteinase activity in cardiac fibroblasts in vitro. Circ Res. 2000; 86:1259–1265. [PubMed: 10864917]
27. Hwang MW, Matsumori A, Furukawa Y, Ono K, Okada M, Iwasaki A, Hara M, Miyamoto T, Touma M, Sasayama S. Neutralization of interleukin-1beta in the acute phase of myocardial infarction promotes the progression of left ventricular remodeling. J Am Coll Cardiol. 2001; 38:1546–1553. [PubMed: 11691538]
28. Frangogiannis NG. Regulation of the inflammatory response in cardiac repair. Circ Res. 2012; 110:159–173. [PubMed: 22223212]
29. Dobaczewski M, Xia Y, Bujak M, Gonzalez-Quesada C, Frangogiannis NG. CCR5 signaling suppresses inflammation and reduces adverse remodeling of the infarcted heart, mediating recruitment of regulatory T cells. Am J Pathol. 2010; 176:2177–2187. [PubMed: 20382703]
30. Chan W, Taylor AJ, Ellims AH, Lefkovits L, Wong C, Kingwell BA, Natoli A, Croft KD, Mori T, Kaye DM, Dart AM, Duffy SJ. Effect of iron chelation on myocardial infarct size and oxidative stress in ST-elevation-myocardial infarction. Circ Cardiovasc Interv. 2012; 5:270–278. [PubMed: 22496085]
31. Seropian IM, Toldo S, Van Tassell BW, Abbate A. Anti-inflammatory strategies for ventricular remodeling following ST-segment elevation acute myocardial infarction. J Am Coll Cardiol. 2014; 63:1593–1603. [PubMed: 24530674]
32. Wei S, Guo A, Chen B, Kutschke W, Xie YP, Zimmerman K, Weiss RM, Anderson ME, Cheng H, Song LS. T-tubule remodeling during transition from hypertrophy to heart failure. Circ Res. 2010; 107:520–531. [PubMed: 20576937]

Clinical Perspective

Numerous studies have shown that an important prognostic feature of acute myocardial infarction (AMI) is its size. However, with the advent of late-gadolinium enhancement CMR nearly two decades ago, key studies have revealed that in addition to infarct size, the presence of late/persistent microvascular obstruction (i.e. persistence of acutely obstructed microvasculature within the myocardium despite the restoration of blood flow to the upstream epicardial coronary artery) is also an independent, negative predictor of event-free survival. More recently, meta-analysis studies have further revealed that persistent microvascular obstructions increase the risk of major adverse cardiovascular outcomes, comprising of death or hospitalization for heart failure, by more than four fold compared to infarct size alone. To date, the negative outcomes associated with persistent microvascular obstructions have been tied to the diminished penetrance of macrophages to the infarct core. However, why these infarcts continue to remodel adversely even after the microvascular obstructions are resolved, typically within two weeks post infarction, has not been investigated. In this manuscript, using a clinically relevant large animal model, we demonstrate for the first time that persistent microvascular obstructions, with or without intramyocardial hemorrhage, resolve into ferric iron crystals within the infarcted myocardium. These iron crystals appear to drive a sustained proinflammatory burden and adverse LV remodeling throughout the post infarction period well after the resolution of persistent microvascular obstruction. Our findings suggest that the crystalline iron depositions within the infarction territories may be a novel therapeutic target in decelerating the onset of heart failure in AMI patients with persistent microvascular obstructions.

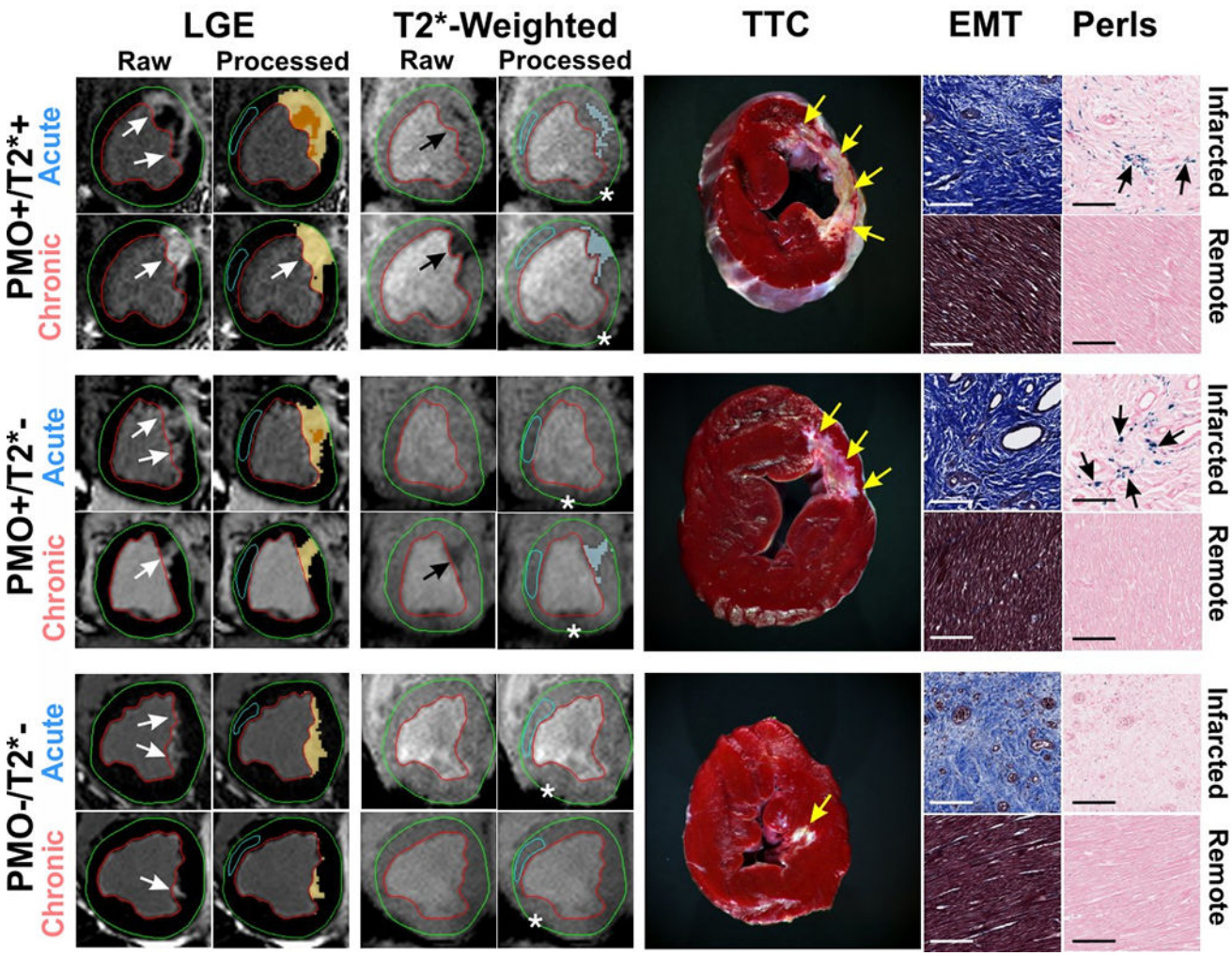

Figure 1. Chronic iron deposition in reperfused myocardial infarctions

Representative in-vivo raw and processed LGE and T2*-weighted images from Reperfused canines acquired in both acute and chronic phases post-MI are shown. Arrows point to the sites of MI and iron deposition on LGE and T2*-weighted images respectively. Corresponding ex-vivo histological sections stained with TTC, EMT and Perls stain are also shown. Scale bars in the microscopic histology images correspond to 50μm. Note the significant chronic iron deposition in the $PMO^{+}/T2^{*-}$ group, despite the absence of acute reperfusion hemorrhage. Perls stain confirmed the presence of chronic iron deposition (blue deposits pointed at by the arrows) in the $PMO^{+}/T2^{*+}$ and $PMO^{+}/T2^{*-}$ groups, but not in the $PMO^{-}/T2^{*-}$ group. EMT stains showed significant fibrosis in the infarcted territory compared to a very mild diffuse fibrosis in the remote territory which were not visually evident on LGE. Asterisks in the T_2*-weighted images point to the sites of off-resonance artifacts that were manually excluded in the final analysis.

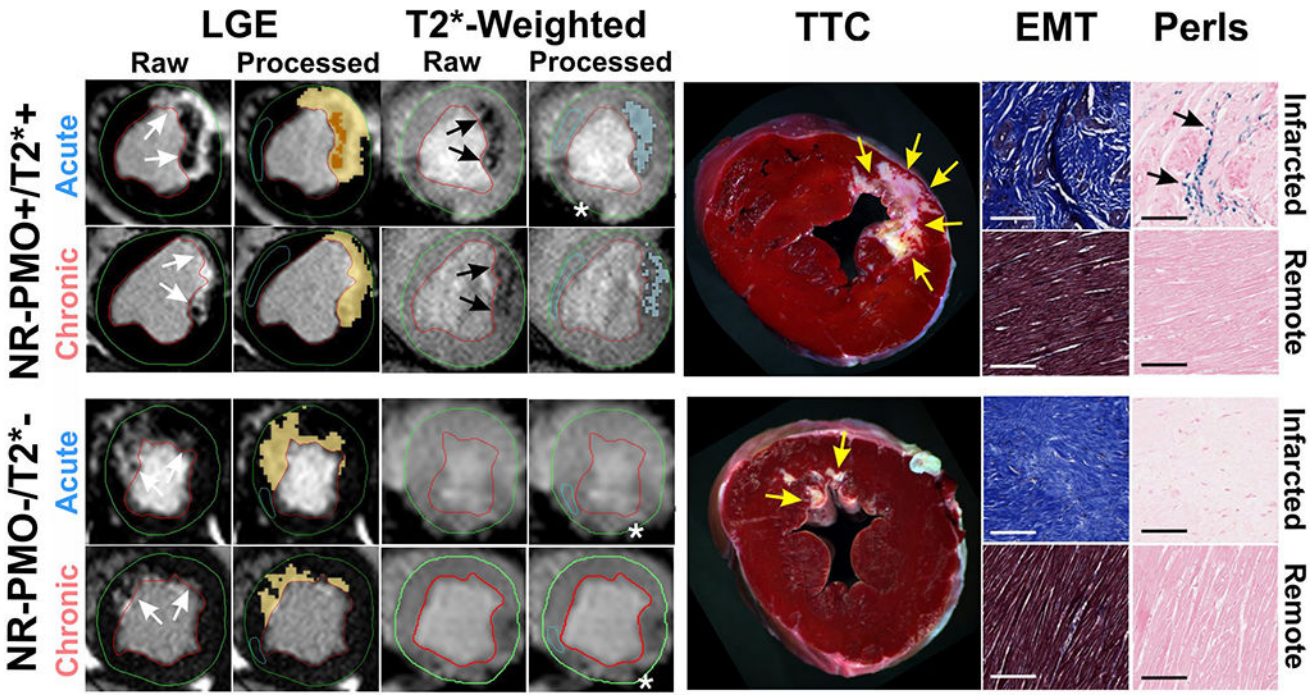

Figure 2. Chronic iron deposition in non-reperfused myocardial infarctions

Representative in-vivo raw and processed LGE and T2*-weighted images from Non-reperfused canines acquired in both acute and chronic phases post-MI are shown. Arrows point to the sites of MI and iron deposition on LGE and T2*-weighted images respectively. Corresponding ex-vivo histological sections stained with TTC, EMT, and Perls stain are also shown. Scale bars in the microscopic histology images correspond to 50μm. Note the significant chronic iron deposition in the NR-PMO^{+}/T2*$^{+}$ group as observed on the in-vivo T2*-weighted images. Perls stain confirmed the presence of chronic iron deposition (blue deposits pointed at by the arrows) in the NR-PMO^{+}/T2*$^{+}$ group, but not in the NR-PMO^{-}/T2*$^{-}$ group. Similar to the reperfused MI, EMT stains showed significant fibrosis in the infarcted territory compared to a very mild diffuse fibrosis in the remote territory, which were not visually evident on LGE. Asterisks in the T2*-weighted images point to the sites of off-resonance artifacts that were manually excluded in the final analysis.

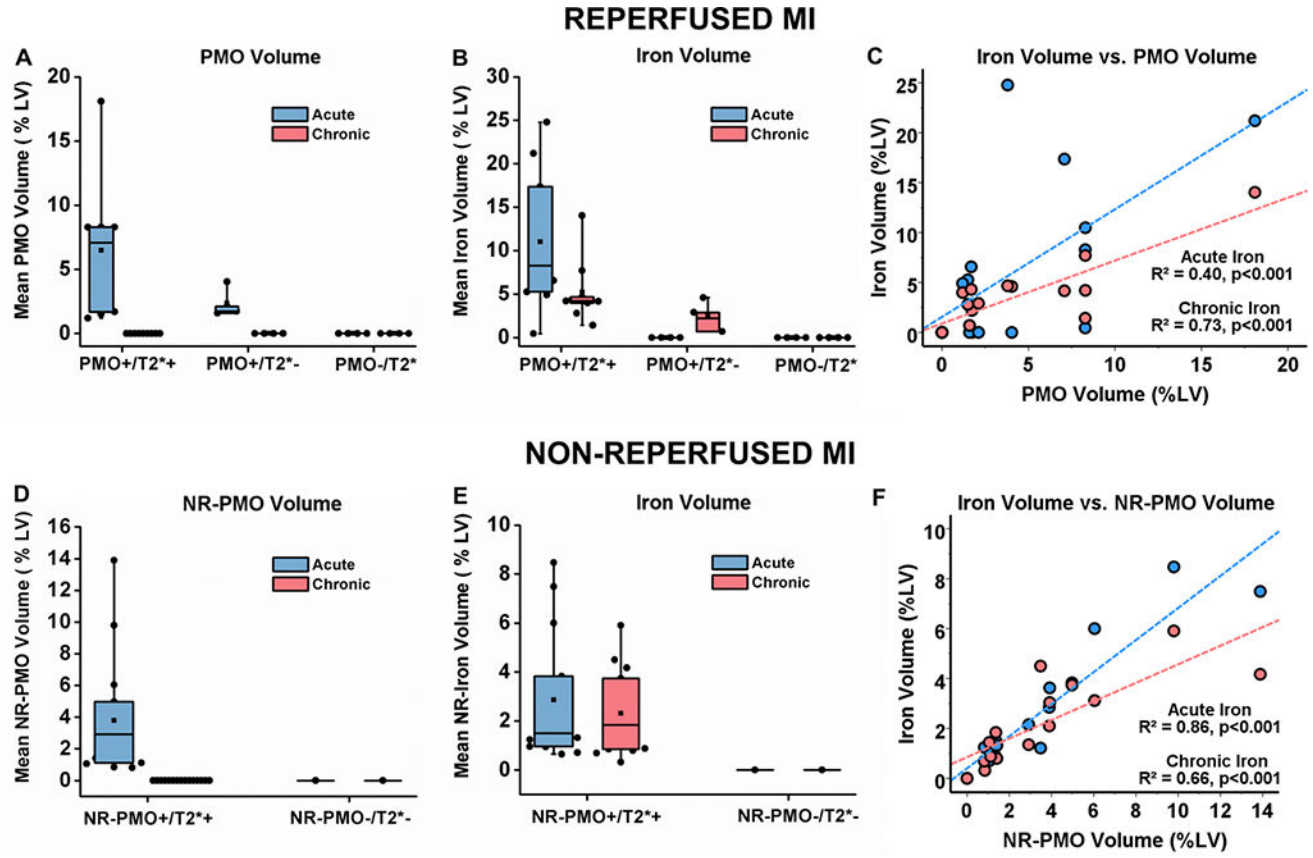

Figure 3. PMO, and iron volumes in reperfused and non-reperfused myocardial infarctions

Median PMO volume (%LV, **A**), iron volume (%LV, **B**), and relationships between PMO volume with acute and chronic iron volumes (**C**) are shown from canines with reperfused MIs ($PMO^{+}/T2^{*+}$: n=9; $PMO^{+}/T2^{*-}$: n=4; $PMO^{-}/T2^{*-}$: n=4). Similarly, median NR-PMO volume (%LV, **D**), iron volume (%LV, **E**), and relationships between PMO volume with acute and chronic iron volumes (**F**) are shown from canines with non-reperfused MIs (NR-$PMO^{+}/T2^{*+}$: n=15; NR-$PMO^{-}/T2^{*-}$: n=1).

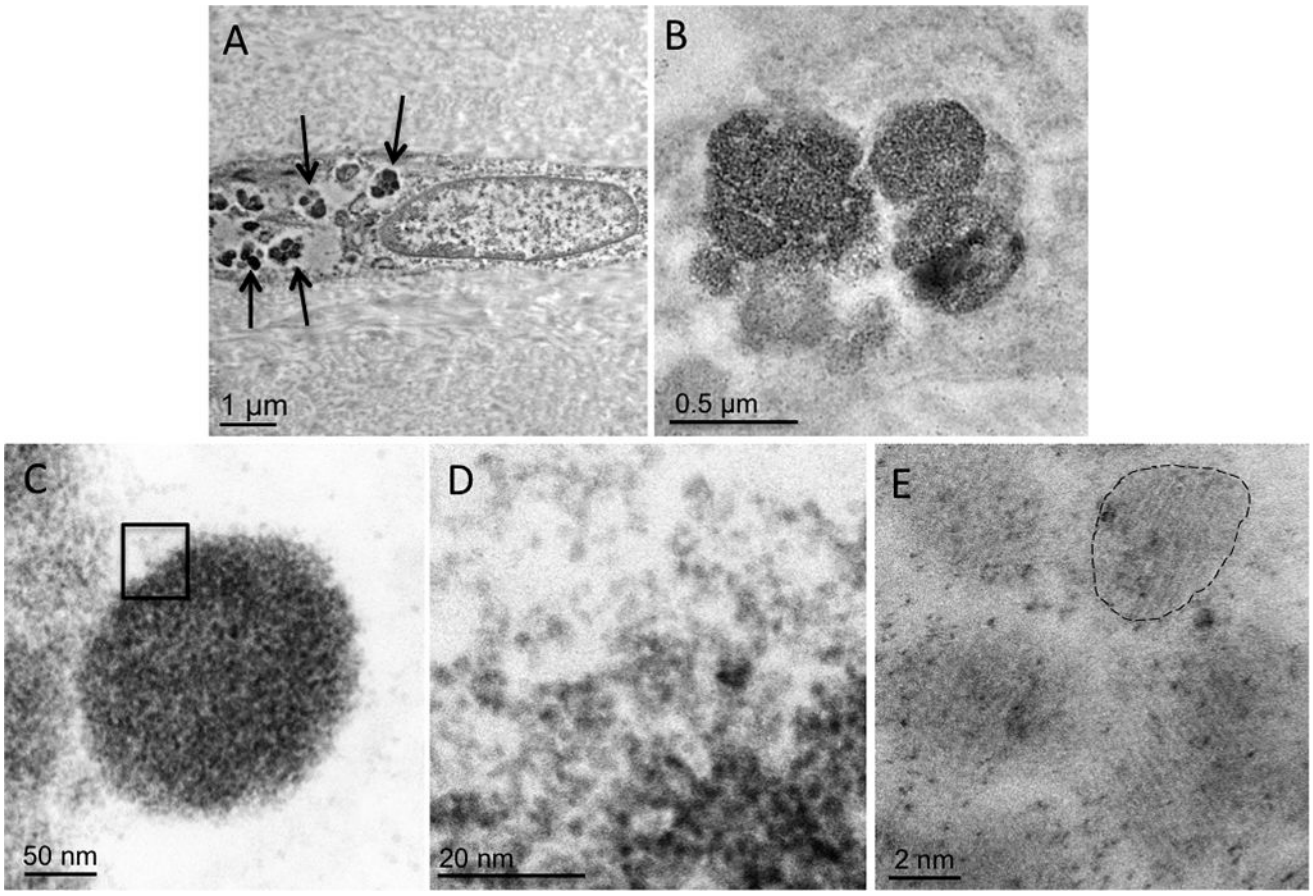

Figure 4. Transmission Electron Microscopy Images of Crystalline Deposits within Macrophages Found in the Territories of Chronic Myocardial Infarction

Panel **A** shows a longitudinal section of the macrophage cell with pronounced intracellular electron-dense material deposits (arrows). Panels **B** and **C** show enlarged area of a typical nodular pattern of material deposition. Panel **D** shows that the nodules are composed of clusters of highly crystalline nanoparticles with an approximate diameter of 2.5 nm (Panel **E**).

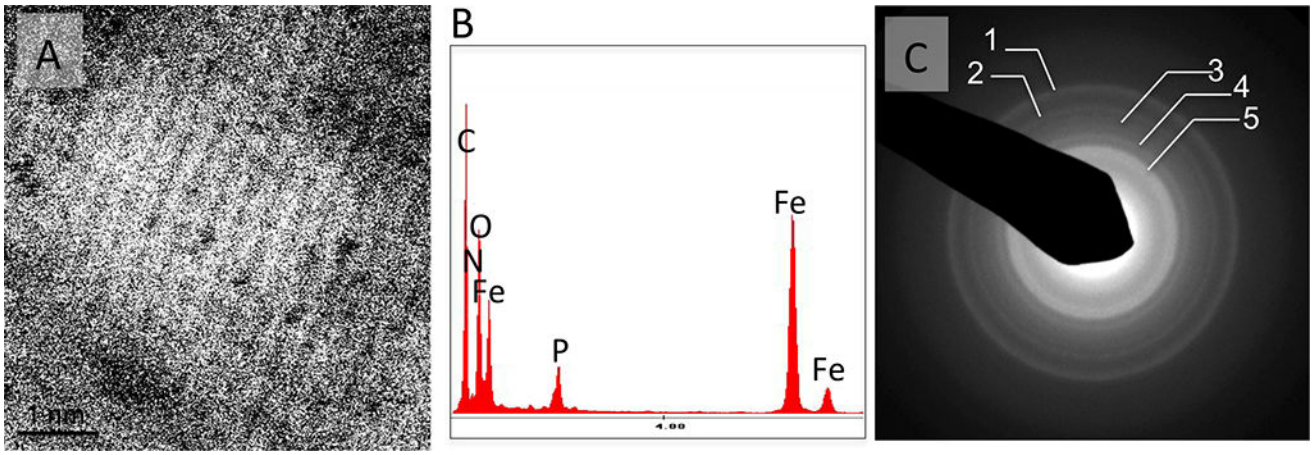

Figure 5. Physicochemical Characterization of Crystalline Iron within Macrophages

Panel **A** shows atomic resolution STEM image of a representative nanocrystalline particle from a Fe nodular cluster in a macrophage intracellular space. Notice the highly ordered pattern of aligned atomic columns. Panel **B** shows the EDS spectrum of the nodular material with the strong Fe presence. Panel **C** shows a SAED obtained from the Fe nodules revealing an exact fit with the pattern of a 6-line ferrihydrite[12]. The respective values of diffraction rings are: 1) 0.150 nm, 2) 0.176 nm, 3) 0.214 nm, 4) 0.226 and 5) 0.256 nm.

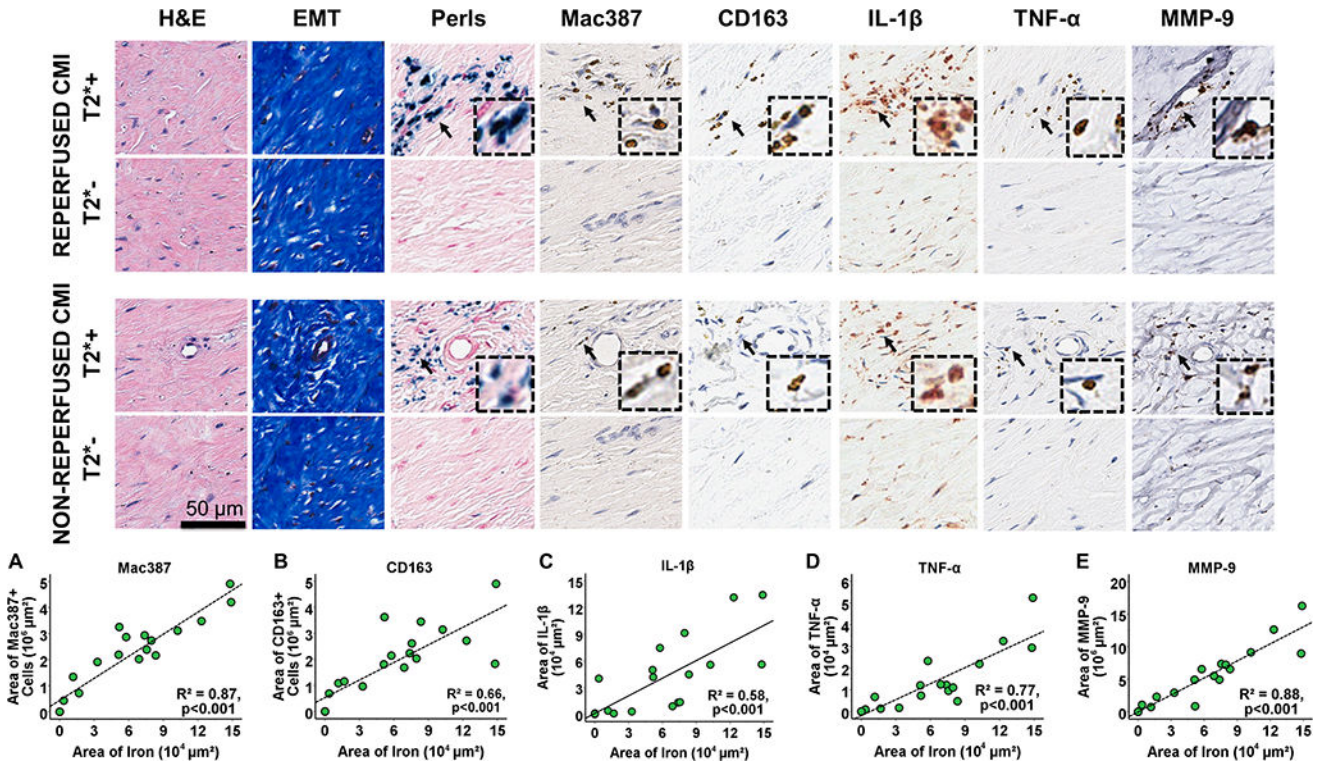

Figure 6. Relationship between pro-inflammatory burden and chronic iron deposition

Representative contiguous ex-vivo histology sections stained with EMT, Perls, and monoclonal antibodies for Mac387, CD163, IL-1β, TNF-α and MMP-9 are shown from canines with reperfused and non-reperfused MIs with and without T2* losses (T2*+ and T2*- respectively) as observed in ex-vivo T2*-weighted images. Note significant co-localization of Mac387+ cells, TNF-α activity, and MMP-9 activity with chronic iron deposits. Strong linear relationships (n=20) of the area of iron (measured from Perls stain) were observed with area of Mac387+ cells (**A**), area of CD163+ cells (**B**), area of IL-1β activity (**C**), area of TNF-α activity (**D**), and area of MMP-9 activity (**E**). Arrows indicate the presence of specific markers of interest, which are zoomed in (insets).

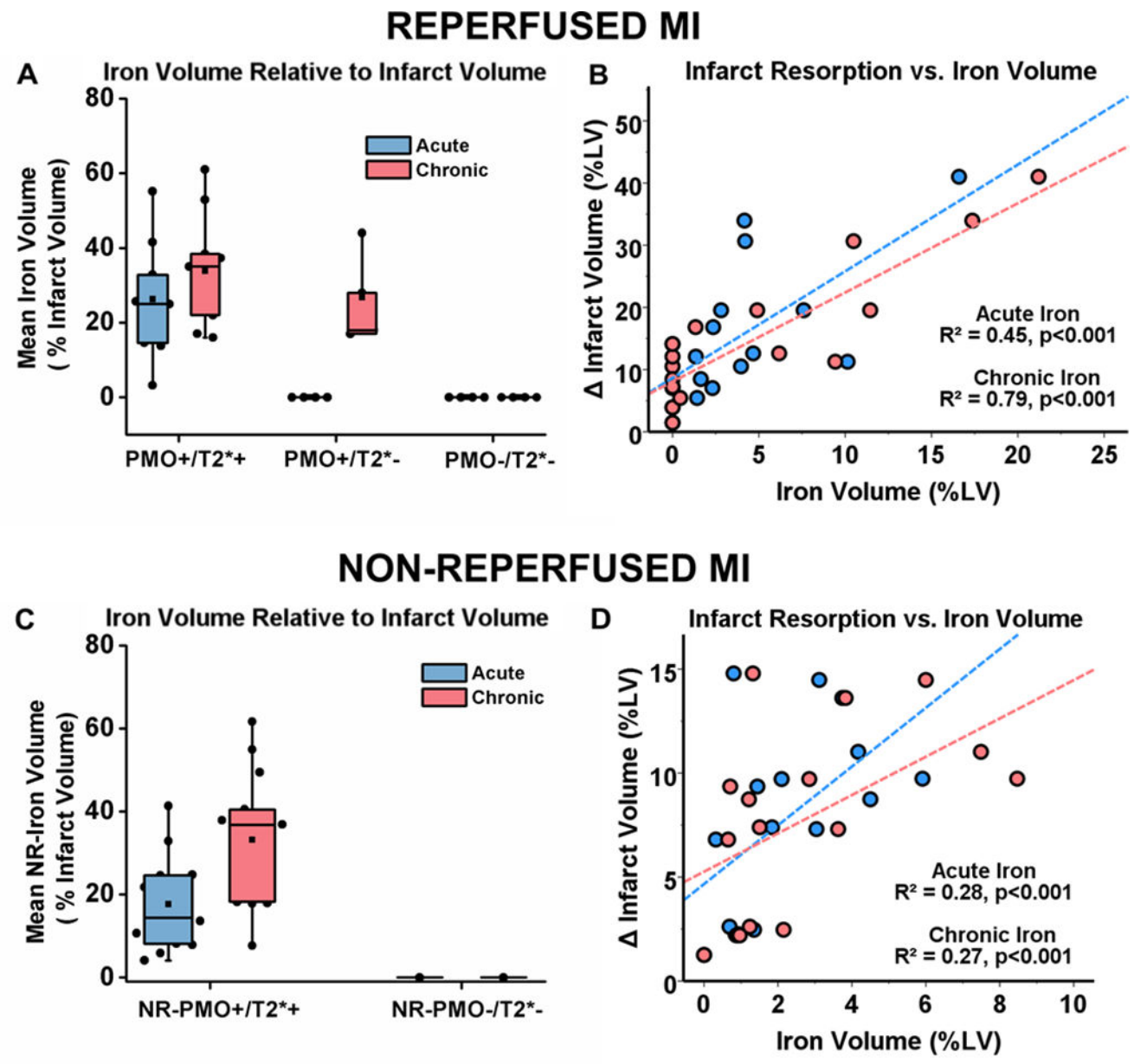

Figure 7. Relationship between iron volume and infarct remodeling in reperfused and non-reperfused myocardial infarctions

Median iron volume as a fraction of infarct volume in acute and chronic phases of infarctions is shown in panels **A** (reperfused MI) and **C** (non-reperfused MI). The relationship between infarct resorption as a function of acute and chronic iron volumes are shown in panel **B** (non-reperfused MI) and **D** (non-reperfused MI). Sample sizes for the different reperfused and non-reperfused groups are as follows: i) Reperfused MIs – $PMO^{+}/T2^{*+}$: n=9; $PMO^{+}/T2^{*-}$: n=4; $PMO^{-}/T2^{*-}$: n=4, ii) Non-Reperfused MIs – NR-$PMO^{+}/T2^{*+}$: n=15; NR-$PMO^{-}/T2^{*-}$: n=1.

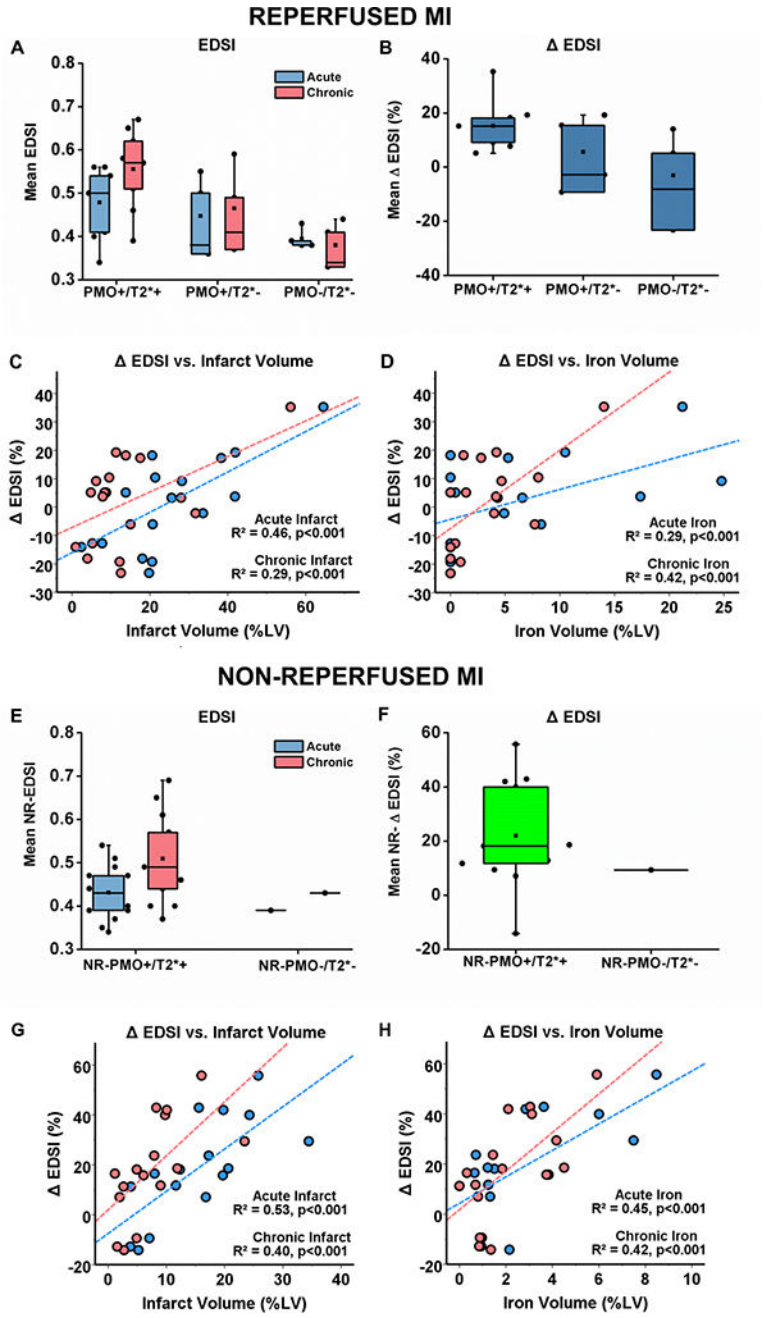

Figure 8. Relationship between Iron Volume and LV Structural Remodeling in reperfused and non-reperfused myocardial infarctions

Median EDSI from reperfused MIs (**A**) and non-reperfused MIs (**E**), as well as ΔEDSI from reperfused MIs (**B**) and non-reperfused MIs (**F**). Significant linear relationships of ΔEDSI with both acute and chronic infarct volumes were observed in both reperfused (**C**) and non-reperfused MIs (**G**). Similarly, significant linear relationships of ΔEDSI with acute and chronic iron volumes were evident in both reperfused (**D**) and non-reperfused (**H**) MIs. Sample sizes for the different reperfused and non-reperfused groups are as follows: i)

Reperfused MIs – $PMO^{+}/T2^{*+}$: n=9; $PMO^{+}/T2^{*-}$: n=4; $PMO^{-}/T2^{*-}$: n=4, ii) Non-Reperfused MIs – NR-$PMO^{+}/T2^{*+}$: n=15; NR-$PMO^{-}/T2^{*-}$: n=1.